Journal of Machine Engineering, 2025, Vol. 25
ISSN 1895-7595 (Print) ISSN 2391-8071 (Online)

Received*: 20 March 2025* / Accepted: *04 September 2025* / Published online: *09 September 2025*

bidirectional DC/DC converter,
PI and fuzzy logic controllers,
vehicle-to-grid, grid-to-vehicle

Hamza EL-HASSOUNI[1*], Abdelaziz FRI[1],
Rachid EL BACHTIRI[1], Karima EL HAMMOUMI[1]

PERFORMANCE EVALUATION OF PI AND FUZZY LOGIC CONTROLLERS FOR A BIDIRECTIONAL BUCK-BOOST DC/DC CONVERTER IN V2G AND G2V APPLICATIONS

This paper presents a comparative analysis of a linear proportional-integral controller and a nonlinear fuzzy logic controller for a bidirectional buck-boost converter in onboard chargers for vehicle-to-grid and grid-to-vehicle applications. The study examines the robustness of both control strategies under voltage variations and assesses their dynamic response to setpoint changes. Simulation results highlight the advantages and limitations of each controller in terms of stability, transient behaviour, and adaptability to varying operating conditions. The findings provide insights into selecting the most effective control approach for enhancing the performance and reliability of bidirectional power conversion in electric vehicle charging systems.

1. INTRODUCTION

Electrifying the transportation sector presents a compelling solution to pressing environmental and public health challenges. By reducing reliance on traditional internal combustion engine (ICE) vehicles, electric vehicles (EVs) emerge as a cleaner and more sustainable alternative, paving the way for a greener and healthier future [1]. EVs with advanced energy storage systems have gained attention as potential alternative energy sources. Moreover, researchers advocate for utilizing EVs in stationary applications, as they remain parked for a large time of the day. Using EVs as mobile power plants enables bidirectional energy flow between vehicles, homes, and the grid [2]. This approach enhances system flexibility, improves efficiency, and helps maintain energy balance [3]. To promote the integration of EVs as mobile power plants, providing electrical energy from EVs to the grid at opportune times provides numerous important benefits, including improved grid

[1] Laboratory of Innovative Technology and Computer Science, Higher School of Technology, Sidi Mohamed Ben Abdellah University, Morocco
[*] E-mail: hamza.elhassouni3@usmba.ac.ma
https://doi.org/10.36897/jme/210294

stability and reduced peak demand [2]. This is known as vehicle-to-grid (V2G). Conversely, charging EVs from the grid is referred to grid-to-vehicle (G2V) concept [4]. Additionally, EV can supply energy directly to homes or buildings in a stand-alone mode without connecting to the main power grid, this is known as vehicle to home (V2H) [5]. Figure 1 depicts all potential strategies for providing energy from EVs.

To enable the charging and discharging of EV batteries, two main types of chargers are utilized: onboard and off-board chargers. Onboard chargers can be designed as unidirectional/bidirectional, single-stage/multi-stage systems and may be categorized as integrated or non-integrated configurations [2, 6, 7]. This paper focuses on the two-stage bidirectional onboard charger, which consists of a bidirectional AC/DC converter connected to a bidirectional DC/DC converter, with particular emphasis on the bidirectional DC/DC converter as shown in Fig. 2.

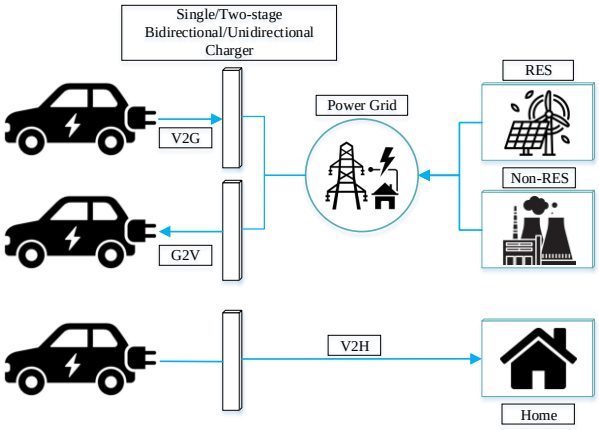

Fig. 1. Strategies for delivering energy from EVs that are viable. V2G, G2V, and V2H (RES: Renewable Energy Sources)

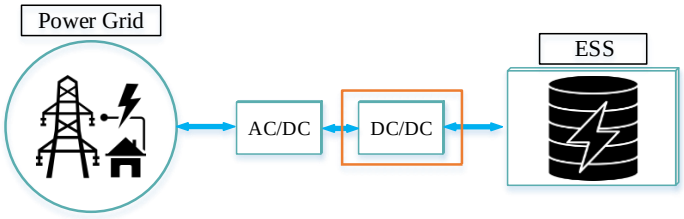

Fig. 2. Two stage bidirectional onboard charger block diagram

As highlighted in various studies, commonly used bidirectional DC/DC converters in onboard chargers for V2G and G2V applications include non-isolated types such as buck-boost and interleaved converters, which are favoured for their simplicity and efficiency. On the other hand, isolated topologies like the dual active bridge, dual active half-bridge, CLLC, and LCL resonant converters are preferred for their high efficiency and galvanic isolation [8–10]. To control those converters, the commonly used strategies include proportional-integral-derivative (PID) control, sliding mode control, dynamic evolution control, model predictive control, fuzzy logic control (FLC), digital control, and boundary control, as reported in studies [9, 11, 12].

In this study focuses on the non-isolated bidirectional buck-boost DC/DC converter and analyse its performance under two different control strategies: the conventional PI controller, classified as a linear control method, and the FLC, which represents a nonlinear approach. While numerous studies [13–16] have compared the performance of PI and FLC in unidirectional converters such as buck, boost, and buck-boost topologies, limited research has been conducted on their application in bidirectional converters. Given the growing importance of bidirectional power flow in applications such as EVs and renewable energy systems, this study aims to provide a comprehensive performance comparison of PI and FLC in a bidirectional topology. Unlike previous works, this work highlights the novelty of evaluating both buck and boost modes with multiple performance indices, providing a more comprehensive comparison for practical bidirectional applications. The results will contribute to a better understanding of the advantages and limitations of each controller, offering insights for optimizing the control strategy of bidirectional DC/DC converters in practical applications.

2. PRESENTATION OF THE BIDIRECTIONAL BUCK-BOOST DC/DC CONVERTER

Non-isolated bidirectional DC/DC converters (BDC) rely on an inductor as the energy transfer unit to facilitate power transfer between the source and the load. These topologies are more cost-effective than isolated DC/DC due to the absence of a high-frequency transformer. Additionally, they feature fewer switches and passive components, simplifying the design and reducing overall costs [17]. However, non-isolated topologies fall short of meeting safety standards, which limits their applicability in certain scenarios. Furthermore, they offer a narrower voltage conversion range, a more restricted soft-switching range, and reduced control complexity compared to isolated topologies [18]. The buck-boost converter is the most widely used non-isolated topology. In this configuration, the BDC functions as a boost converter during V2G operation and a buck converter during G2V operation [8, 9]. The topology chosen comprises two bidirectional switches (S1 and S2), which are typically realized using MOSFETs or IGBTs. It also includes a DC bus capacitor C1, an output capacitor C2, and an inductor L as shown in Fig. 3.

The inductor L, the DC bus capacitor C1, the output capacitor C2 can be calculated using equations 1, 2, and 3 respectively.

$$L = \frac{(V_{dc} - V_{bat}) \,.\, D}{\Delta I_L \,.\, f_{sw}} \tag{1}$$

$$C_1 = \frac{I_{out} \,.\, D}{\Delta V_{dc} \,.\, f_{sw}} \tag{2}$$

$$C_2 = \frac{(1 - D) \,.\, V_{bat}}{8L \,.\, \Delta V_{bat} \,.\, {f_{sw}}^2} \tag{3}$$

The duty cycle associated with each mode is given in the equations 4 and 5:

$$D(buck\ mode) = \frac{V_{bat}}{V_{dc}} \tag{4}$$

$$D(boost\ mode) = \frac{V_{dc} - V_{bat}}{V_{dc}} \tag{5}$$

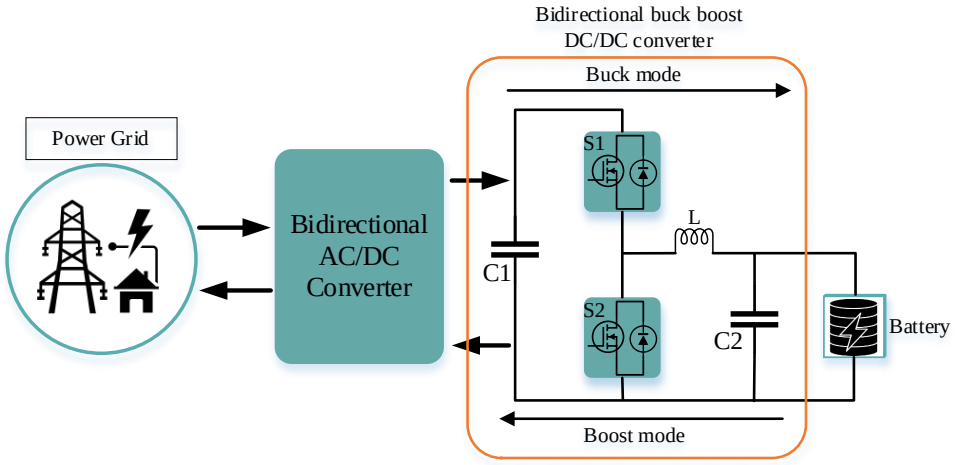

Fig. 3. Bidirectional buck-boost topology: buck and boost modes direction

2.1. STATE-SPACE MODELLING FOR BUCK MODE

In buck mode, the converter steps down V_{dc} to V_{bat}. During this mode, S_1 is actively switched while S_2 remains off. When S_1 is ON, current flows from V_{dc} through S_1 and the inductor L to charge the battery. When S_1 is OFF, the inductor's stored energy maintains the current flow, which passes through the body diode of S_2 to continue charging the battery. The equivalent circuits for buck mode, when S_1 is ON and OFF, are illustrated in Fig. 4.

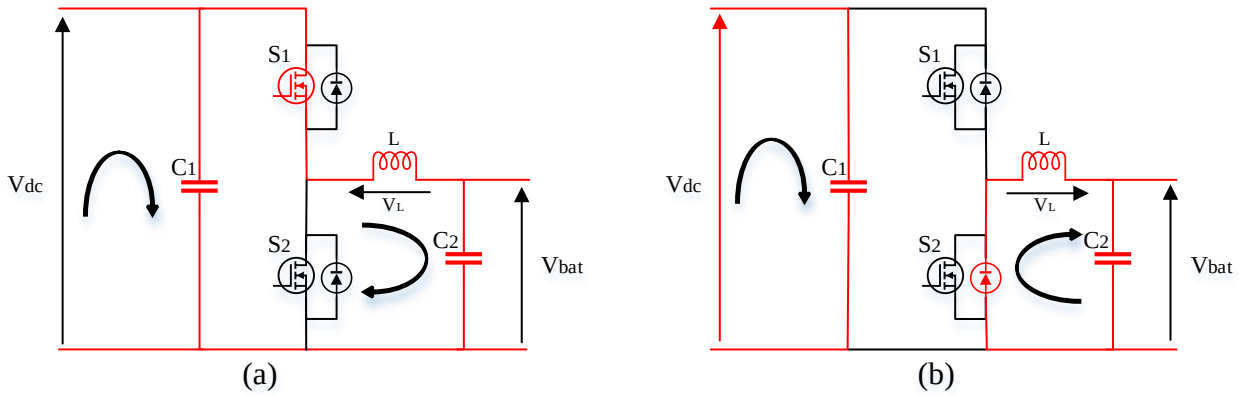

Fig. 3. Buck mode: (a) when S_1 is ON, (b) when S_1 is OFF

To model the buck mode of this converter, state-space modelling was used, it consists of two equations: the state equation and the output equation, as shown in the equations 6 and 7 respectively.

$$\dot{x} = A\,x(t) + B\,u(t) \tag{6}$$

$$\mathrm{y(t)} = \mathrm{C\ x(t)} + \mathrm{D\ u(t)} \tag{7}$$

In this mode the state variables are $x_1(t) = i_L(t)$ and $x_2(t) = V_{C2}(t)$.

In the first period, when S_1 is ON, Kirchhoff's rules are applied to obtain (8). Where R_{buck} is the output load during buck mode, and r_{S1} and r_L are the switch resistance and inductance resistance, respectively.

$$\begin{cases} \dfrac{di_L(t)}{dt} = \dfrac{V_{dc}(t)}{L} - \dfrac{V_{C2}(t)}{L} - \dfrac{(r_{S1} + r_L)}{L} i_L(t) \\ \dfrac{dV_{C2}(t)}{dt} = \dfrac{i_L(t)}{C_2} - \dfrac{V_{C2}(t)}{R_{buck}C_2} \end{cases} \tag{8}$$

Using (8) the state-space representation will be as shown in (9).

$$\begin{bmatrix} \dfrac{di_L(t)}{dt} \\ \dfrac{dV_{C2}(t)}{dt} \end{bmatrix} = \begin{bmatrix} -\dfrac{(r_{S1} + r_L)}{L} & -\dfrac{1}{L} \\ \dfrac{1}{C_2} & -\dfrac{1}{R_{buck}C_2} \end{bmatrix} \begin{bmatrix} i_L(t) \\ V_{C2}(t) \end{bmatrix} + \begin{bmatrix} \dfrac{1}{L} \\ 0 \end{bmatrix} V_{dc}(t)$$
$$V_{bat}(t) = [0 \quad 1] \begin{bmatrix} i_L(t) \\ V_{C2}(t) \end{bmatrix} + [0]\, V_{dc}(t) \tag{9}$$

In the second period, S_1 is OFF and the current passes through the body diode of S_2 resulting in (10).

$$\begin{cases} \dfrac{di_L(t)}{dt} = -\dfrac{V_{C2}(t)}{L} - \dfrac{r_L}{L} i_L(t) \\ \dfrac{dV_{C2}(t)}{dt} = \dfrac{i_L(t)}{C_2} - \dfrac{V_{C2}(t)}{R_{buck}C_2} \end{cases} \tag{10}$$

Using (10), the state-space representation given as follows (11).

$$\begin{bmatrix} \dfrac{di_L(t)}{dt} \\ \dfrac{dV_{C2}(t)}{dt} \end{bmatrix} = \begin{bmatrix} -\dfrac{r_L}{L} & -\dfrac{1}{L} \\ \dfrac{1}{C_2} & -\dfrac{1}{R_{buck}C_2} \end{bmatrix} \begin{bmatrix} i_L(t) \\ V_{C2}(t) \end{bmatrix} + \begin{bmatrix} 0 \\ 0 \end{bmatrix} V_{dc}(t)$$
$$V_{bat}(t) = [0 \quad 1] \begin{bmatrix} i_L(t) \\ V_{C2}(t) \end{bmatrix} + [0]\, V_{dc}(t) \tag{11}$$

Based on linearization theory, and by introducing perturbation, the system will be split into a DC component and an AC component as shown in (12).

$$\begin{gathered} x(t) = X + \hat{x}(\mathrm{t}) \\ V_{bat}(t) = V_{bat} + \widehat{v_{bat}}(t) \\ V_{dc}(t) = V_{dc} + \widehat{v_{dc}}(t) \\ d(t) = D + \hat{d}(t) \end{gathered} \tag{12}$$

In this mode, the input voltage is considered constant, which means that $\widehat{v_{dc}}(t)$=0. By substituting these signals into the average state-space equations, (13) and (14) are obtained.

$$\begin{aligned} \frac{d\hat{x}(\mathrm{t})}{dt} = {} & AX + BV_{dc} + A\hat{x}(\mathrm{t}) + \left[X\left(A_{on} - A_{off}\right) + V_{dc}\left(B_{on} - B_{off}\right)\right]\hat{d}(t) \\ & + \left(A_{on} - A_{off}\right)\hat{x}(\mathrm{t})\hat{d}(t) \end{aligned} \tag{13}$$

$$V_{bat} + \widehat{v_{bat}}(t) = CX + C\hat{x}(\mathrm{t}) + X\left(C_{on} - C_{off}\right)\hat{d}(t) + \left(C_{on} - C_{off}\right)\hat{x}(\mathrm{t})\hat{d}(t) \tag{14}$$

Where A, B, and C matrices are equal to:

$$\begin{gathered} A = DA_{on} + (1-D)A_{off} \\ B = DB_{on} + (1-D)B_{off} \\ C = DC_{on} + (1-D)C_{off} \end{gathered} \tag{15}$$

By neglecting the second-order AC term and keeping only the first-order AC term [19], and knowing that $A_{on} \neq A_{off}$, $B_{on} \neq B_{off}$, $C_{on} = C_{off}$, the extracted small-signal transfer function in the Laplace domain is shown in (16).

$$\frac{\widehat{v_{bat}}(s)}{\hat{d}(s)} = C(sI - A)^{-1}\left[X\left(A_{on} - A_{off}\right) + V_{dc}\left(B_{on} - B_{off}\right)\right] \tag{16}$$

Where C and A are defined in (15), I is an identity matrix, and X is the DC term (V_{bat} and I_L). The final small signal transfer function for boost mode, based on the parameters provided in Table 1, is expressed as follows:

$$TF_{buck}(s) = \frac{\widehat{v_{bat}}(s)}{\hat{d}(s)} = \frac{798400s + 7.984\ 10^7}{s^2 + 700s + 2.006\ 10^7} \tag{17}$$

2.2. STATE-SPACE MODELLING FOR BOOST MODE

In boost mode, the converter steps up V_{bat} to V_{dc}. Here, S_2 is actively switched while S_1 remains off. When S_2 is ON, the inductor stores energy from the battery. When S_2 is OFF, the energy stored in the inductor is released, causing current to flow through the body diode of

S1 to the input of the bidirectional AC/DC linked to the grid. The equivalent circuits for boost mode, when S_2 is ON and OFF, are illustrated in Fig. 5.

For boost mode, the state variables are $x_1(t)=i_L(t)$ and $x_2(t)=V_{C1}(t)$, during the first period, when S_2 is ON and when S_2 is OFF, (18) and (19) are obtained. Where R_{boost} represent the output load during boost mode.

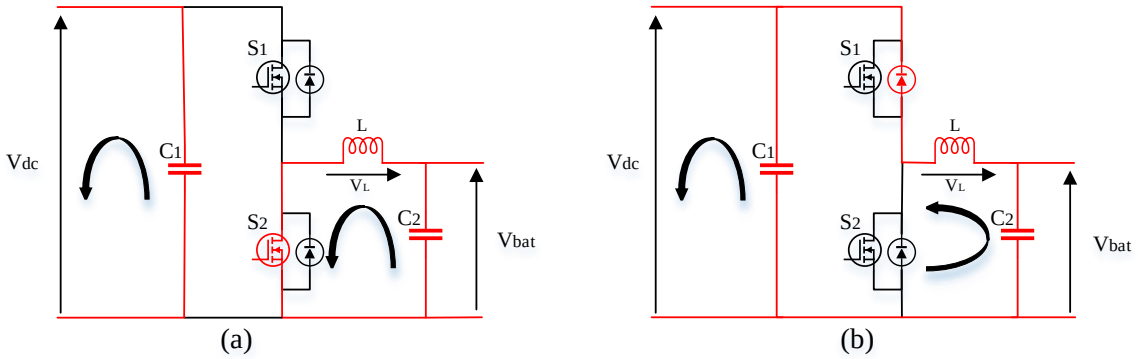

Fig. 4. Boost mode: (a) when S_2 is ON, (b) when S_2 is OFF

$$\begin{cases} \dfrac{di_L(t)}{dt} = \dfrac{V_{bat}(t)}{L} - \dfrac{(r_{S2}+r_L)}{L} i_L(t) \\ \dfrac{dV_{C1}(t)}{dt} = -\dfrac{V_{C1}(t)}{R_{boost}C_1} \end{cases} \tag{18}$$

$$\begin{cases} \dfrac{di_L(t)}{dt} = \dfrac{V_{bat}(t)}{L} - \dfrac{V_{C1}(t)}{L} - \dfrac{r_L}{L} i_L(t) \\ \dfrac{dV_{C1}(t)}{dt} = \dfrac{i_L(t)}{C_1} - \dfrac{V_{C1}(t)}{R_{boost}C_1} \end{cases} \tag{19}$$

Witch gives the state representation when S_2 is ON and OFF, as shown in (20) and (21) respectively.

$$\begin{bmatrix} \dfrac{di_L(t)}{dt} \\ \dfrac{dV_{C1}(t)}{dt} \end{bmatrix} = \begin{bmatrix} -\dfrac{(r_{S2}+r_L)}{L} & 0 \\ 0 & -\dfrac{1}{R_{boost}C_1} \end{bmatrix} \begin{bmatrix} i_L(t) \\ V_{C1}(t) \end{bmatrix} + \begin{bmatrix} \dfrac{1}{L} \\ 0 \end{bmatrix} V_{bat}(t)$$
$$V_{dc}(t) = [0 \quad 1] \begin{bmatrix} i_L(t) \\ V_{C1}(t) \end{bmatrix} + [0] V_{bat}(t) \tag{20}$$

$$\begin{bmatrix} \dfrac{di_L(t)}{dt} \\ \dfrac{dV_{C1}(t)}{dt} \end{bmatrix} = \begin{bmatrix} -\dfrac{r_L}{L} & -\dfrac{1}{L} \\ \dfrac{1}{C_1} & -\dfrac{1}{R_{boost}C_1} \end{bmatrix} \begin{bmatrix} i_L(t) \\ V_{dc}(t) \end{bmatrix} + \begin{bmatrix} \dfrac{1}{L} \\ 0 \end{bmatrix} V_{bat}(t)$$
$$V_{dc}(t) = [0 \quad 1] \begin{bmatrix} i_L(t) \\ V_{dc}(t \end{bmatrix} + [0] V_{bat}(t) \tag{21}$$

By introducing perturbation as mentioned in (12). And considering that the battery voltage is constant, which means that $\widehat{v_{dc}}(t)$=0. The substitution in the state-space equations results in (22) and (23) respectively.

$$\frac{d\hat{x}(\mathrm{t})}{dt} = \mathrm{AX} + BV_{bat} + A\hat{x}(\mathrm{t}) + \left[X\left(A_{on} - A_{off}\right) + V_{bat}\left(B_{on} - B_{off}\right)\right]\hat{d}(t) + \left(A_{on} - A_{off}\right)\hat{x}(\mathrm{t})\hat{d}(t) \tag{22}$$

$$V_{dc} + \widehat{v_{dc}}(t) = CX + C\hat{x}(\mathrm{t}) + X\left(C_{on} - C_{off}\right)\hat{d}(t) + \left(C_{on} - C_{off}\right)\hat{x}(\mathrm{t})\hat{d}(t) \tag{23}$$

Given that $A_{on} \neq A_{off}$, $B_{on} = B_{off}$, $C_{on} = C_{off}$. From (22) and (23), the extracted small-signal transfer function in the Laplace domain is shown in (24).

$$\frac{\widehat{v_{dc}}(s)}{\hat{d}(s)} = C(sI - A)^{-1}(A_{on} - A_{off})X \tag{24}$$

Where C and A are declared in (15). Using the parameters in Table 1, the final small signal transfer function for boost mode is written in (25).

$$TF_{boost}(s) = \frac{\widehat{v_{dc}}(s)}{\hat{d}(s)} = \frac{-6000s + 3.958\,.\,10^{8}}{2s^{2} + 610s + 50600} \tag{25}$$

3. DESIGN OF CONTROL SYSTEMS

3.1. DESIGN OF PI CONTROLLER

PID controller is the preferred control approach due to its simple implementation [11]. The block diagram of this controller is shown in Fig. 6. The control output *U* is given as shown in equation (26). Where *Kp* is the proportional gain, K_i is the integral gain, K_d is the derivative gain, and ε is the error between the actual output and the desired value.

$$U = K_p + K_i \int_0^t \varepsilon\, dt + K_d \frac{d\varepsilon}{dt} \tag{26}$$

PI and PID controllers are classified as linear controllers, while FLC operates as a nonlinear controller. Both linear and nonlinear control methods are employed to regulate the performance of the converter[16]. In this case, PI controller was used, which is known to be challenging to tune [20]. There are several methods and techniques used to tune a PID controller such as Ziegler-Nichols step response method, Chien-Hrones-Reswick method, Approximate MIGO (M – Constrained Integral Gain Optimization) frequency response method, and Loop shaping method [21] [22]. In this case, based on the transfer functions (17) and (25) extracted for each mode, along with the PID Tuner tool in MATLAB, to adjust the

system bandwidth (in rad/s) to optimize the response time and tune the phase margin to enhance robustness. This process allowed the achievement of the best closed-loop response, yielding K_p and K_i values for each mode, as shown in Table 1.

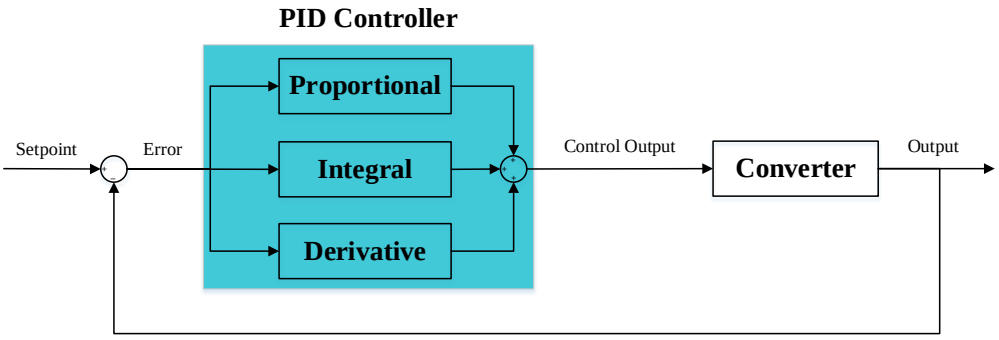

Fig. 5. Block diagram of PID controller

Table 1. PI controller parameters for each mode

	K_p	K_i
Buck Mode	0	2.17975801146447
Boost Mode	0.000349131423452806	0.257704553125067

3.2. DESIGN OF FUZZY LOGIC CONTROLLER

DC/DC converters are nonlinear systems that can be controlled efficiently without the need for a precise mathematical model. To achieve this, FLC is used, which utilizes human-like reasoning to analyse and define system characteristics. Such reasoning can be translated into a structured control framework, referred to as a rule base, which accommodates uncertain inputs. In bidirectional buck-boost systems and other power converters with FLC, there are typically two input signals that are processed: the error signal and the change in error signal as shown in the equations 27 and 28. Where $V_{out}(t)$ is the actual output of the converter and V_{ref} is the desired value. The fuzzy rule is set for these two inputs based on the dynamic behaviour of the error signal [23]. The basic block diagram of FLC for DC/DC converters is shown in Fig. 7.

$$\varepsilon(t) = V_{ref} - V_{out}(t) \tag{27}$$

$$\Delta\varepsilon(t) = \varepsilon(t) - \varepsilon(t - T) \tag{28}$$

FLC comprises four essential components: the fuzzifier, knowledge base, inference system, and defuzzifier [15]. The fuzzifier transforms crisp input values into fuzzy values. The knowledge base includes the rule base, which is built on the principle of IF-THEN statements, and membership functions. Various types of membership functions, such as triangular, trapezoidal, and gaussian, can be employed [24]. The inference system acts as the brain of the controller, converting fuzzy inputs from the fuzzifier into fuzzy outputs based on

the rule base. Finally, the defuzzifier converts the fuzzy output from the inference system into a control signal for the converter.

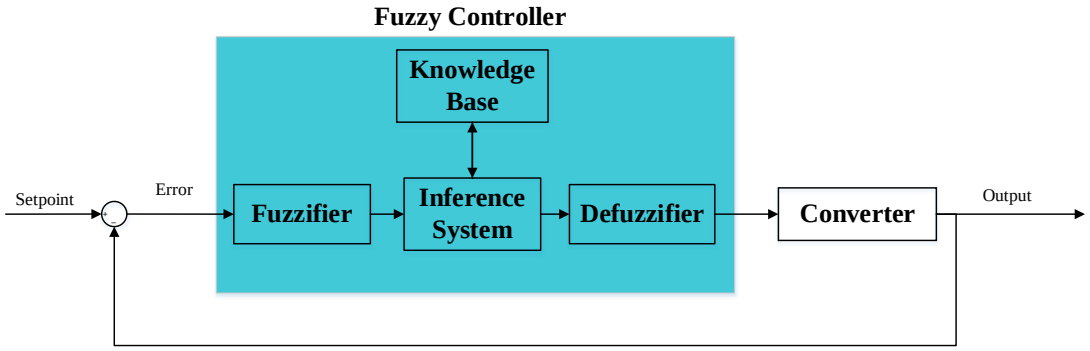

Fig. 6. Fuzzy logic controller block diagram

Several fuzzy inference systems (FIS) are commonly employed in fuzzy logic controllers, including Mamdani and Sugeno FIS [25, 26]. The Sugeno FIS was selected over the Mamdani FIS for this converter application due to its computational efficiency, smooth output generation, and compatibility with adaptive optimization techniques. Unlike Mamdani FIS, which require complex defuzzification, Sugeno's rule consequents use mathematical functions that reduce real-time computational load and improve dynamic response which is critical for power electronics control [27, 28]. The controller's inputs are the error and change in error, which include five membership functions (MFs): Positive Big (PB), Positive Small (PS), Zero (ZE), Negative Small (NS), and Negative Big (NB). There are various forms of MFs, including triangular MF (trimf), trapezoidal MF (trapmf), Gaussian MF (gaussmf), Gaussian 2 MF (gauss2mf), and sigmoidal MF (sigmf). In this case, trapezoidal MF were chosen for the inputs, as illustrated in Fig. 8a. Table 2 shows that twenty-five rules are created from the five MFs for each input. Where D1, D2, D3, D4, and D5 are linear functions and represent the switching duty cycle as shows in (29). The surface graph of the fuzzy system is shown in Fig. 8b.

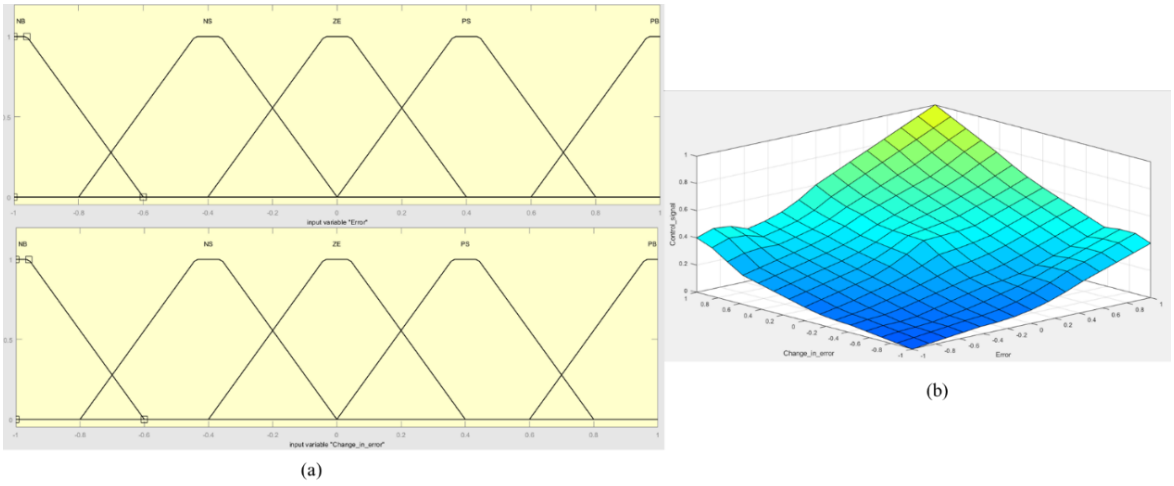

Fig. 7. a) Error and change in error MFs, b) FIS surface graph

Table 2. Fuzzy rule base

Error/Change in Error	NB	NS	ZE	PS	PB
NB	D5	D5	D4	D4	D3
NS	D5	D4	D4	D3	D2
ZE	D4	D4	D3	D2	D1
PS	D4	D3	D2	D2	D1
PB	D3	D2	D2	D1	D1

$$\begin{aligned} D1 &= 0.5\,\varepsilon(t) + 0.5\,\Delta\varepsilon(t) + 0.5 \\ D2 &= 0.4\,\varepsilon(t) + 0.4\,\Delta\varepsilon(t) + 0.4 \\ D3 &= 0.3\,\varepsilon(t) + 0.3\,\Delta\varepsilon(t) + 0.3 \\ D4 &= 0.2\,\varepsilon(t) + 0.2\,\Delta\varepsilon(t) + 0.2 \\ D5 &= 0.1\,\varepsilon(t) + 0.1\,\Delta\varepsilon(t) + 0.1 \end{aligned} \tag{29}$$

4. SIMULATION, RESULT, AND DISCUSSION

The simulation of the proposed converter was performed using MATLAB Simulink. The parameters used for the simulation and for calculating the transfer function in each mode are listed in Table 3. The model-based design of the converter for buck mode and boost mode is shown in Fig. 9.

Table 3. Parameters of the converter used in the simulation

Parameters	Values
V_{dc}	400 V
V_{bat}	300 V
Inductor (L)	0.5 mH
DC capacitor (C1)	1000 uF
Output capacitor (C2)	100 uF
Switching frequency	10 kHz
$r_{S1} = r_{S2}$	0.1 Ohms
r_L	0.25 Ohms

To evaluate each controller, a two-step approach was used. First, V_{dc} was increased from 400 V to 450 V between 1 and 1.5 seconds. Then, V_{dc} decreased from 400 V to 350 V between 2 and 2.5 seconds, while the setpoint of V_{bat} remained constant. This allowed the observation of the converter's behaviour under dynamic changes in V_{dc}. The results obtained using the PI controller and the FLC are presented in Fig. 10 and 11, respectively. When comparing the response of the converter under both controllers, the FLC stands out for its faster response and better handling of voltage variations. It reaches the desired value in 0.38 ms compared to 1.66 ms for the PI controller. More importantly, it settles in 1 ms, whereas the PI controller takes 10 ms to fully stabilize. Both controllers have similar overshoot, with the FLC slightly outperforming the PI controller (4.06% vs. 4.66%). However, the PI controller has a perfect steady-state accuracy, while the FLC holds a small 1 V steady-state error. The real advantage

of the FLC, though, is its robustness when the input voltage fluctuates, it maintains a smooth and stable response, while the PI controller shows small disturbances. The synthesis of the comparison is shown in Table 4.

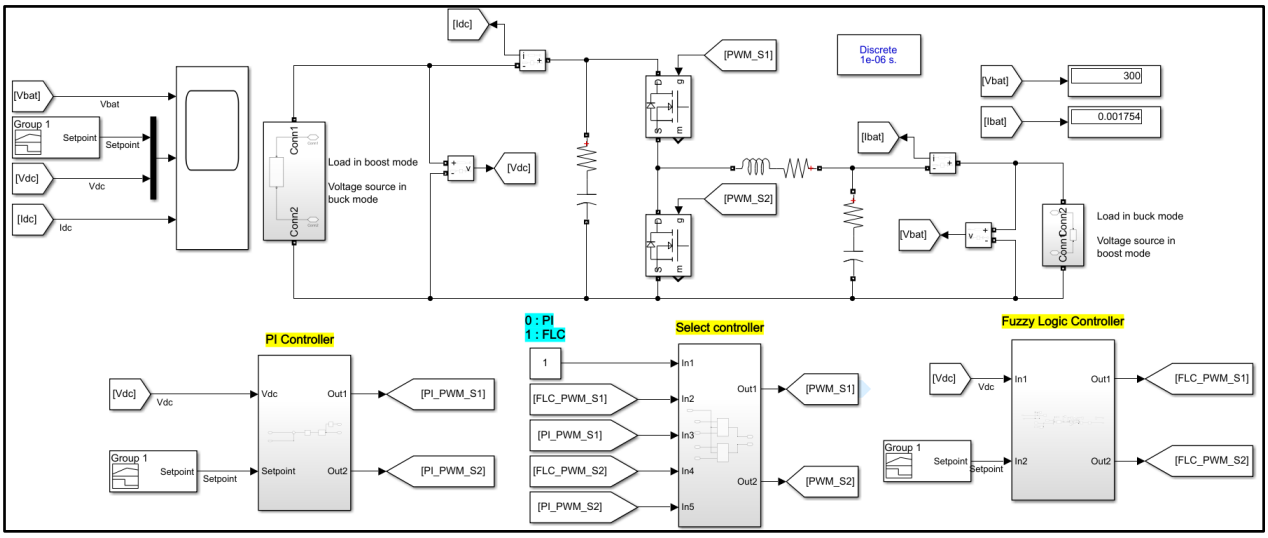

Fig. 8. Model based design of the converter

Table 4. Comparison of PI and fuzzy logic controllers in buck mode

	PI controller	FLC
Rise time (ms)	1.66	0.38
Overshoot (%)	4.66	4.06
Settling time (ms)	10	1
Steady state error (V)	0	1
Robustness to Voltage Sag	Moderate	High

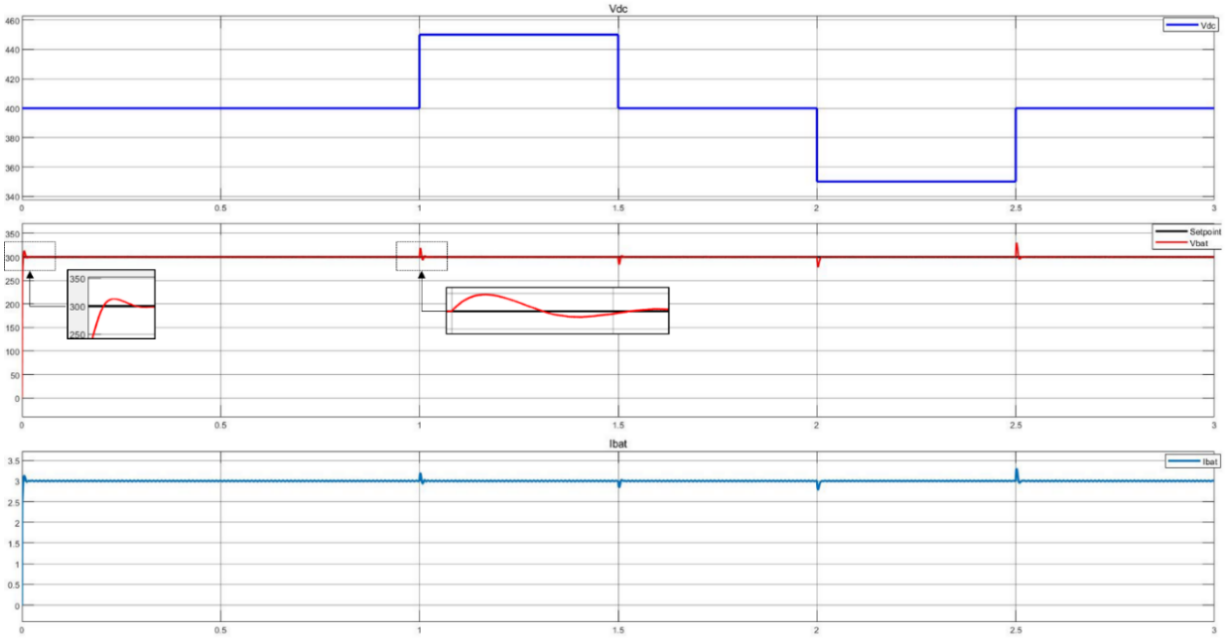

Fig. 9. Result in buck mode under PI controller

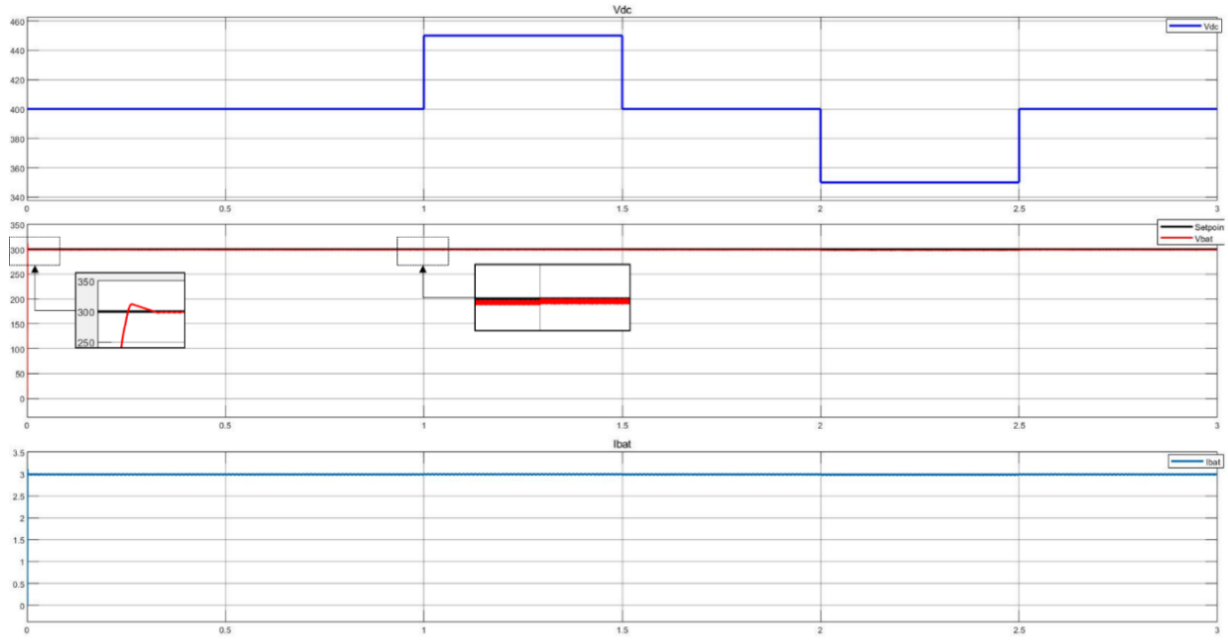

Fig. 10. Result in buck mode under FLC

In order to evaluate the converter in boost mode, the voltage V_{bat} remains constant while the setpoint for the DC voltage V_{dc} varies. Initially, the setpoint is set to 400 V, then it increases to 450 V for 1 second before stabilizing back at 400V. And this allows to evaluate the performance of the controllers under setpoint variations. Figures 12 and 13 illustrate the converter's response using the PI and FL controllers, respectively. The comparison of the performance of the PI controller vs. FLC in the boost mode indicates that the FLC has superior dynamic response and robustness. The rise time is very similar in both controllers with the FLC providing a marginally improved response at 1.13 ms while that for the PI controller is 1.16 ms. However, the FLC reduces overshoot from 19.4% for PI to 14.38%, indicating enhanced stability. The settling time is enhanced most, with the FLC settling at just 15 ms compared to the 77 ms of the PI controller, indicating a much quicker adjustment to steady-state behaviour. The two controllers remain in the same steady-state error of 0V, ensuring precision in voltage regulation. Additionally, the FLC has a higher robustness against setpoint changes, which allows for more stable and efficient operation under various operating conditions, thereby making it a more adaptive and efficient choice for the boost mode of the bidirectional DC/DC converter. Table 5 summarize the result for boost mode.

Table 5. Comparison of PI and fuzzy logic controllers in boost mode

	PI controller	FLC
Rise time (ms)	1.16	1.13
Overshoot (%)	19.4	14.38
Settling time (ms)	77	15
Steady state error (V)	0	0
Robustness to setpoint change	Moderate	High

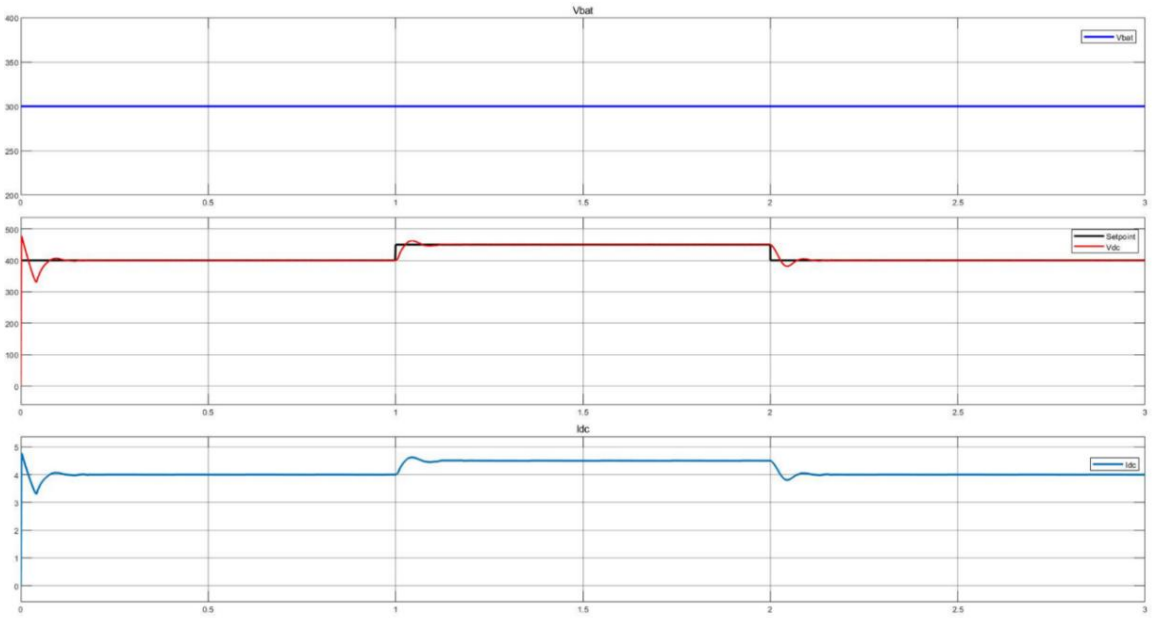

Fig. 11. Result in boost mode under PI controller

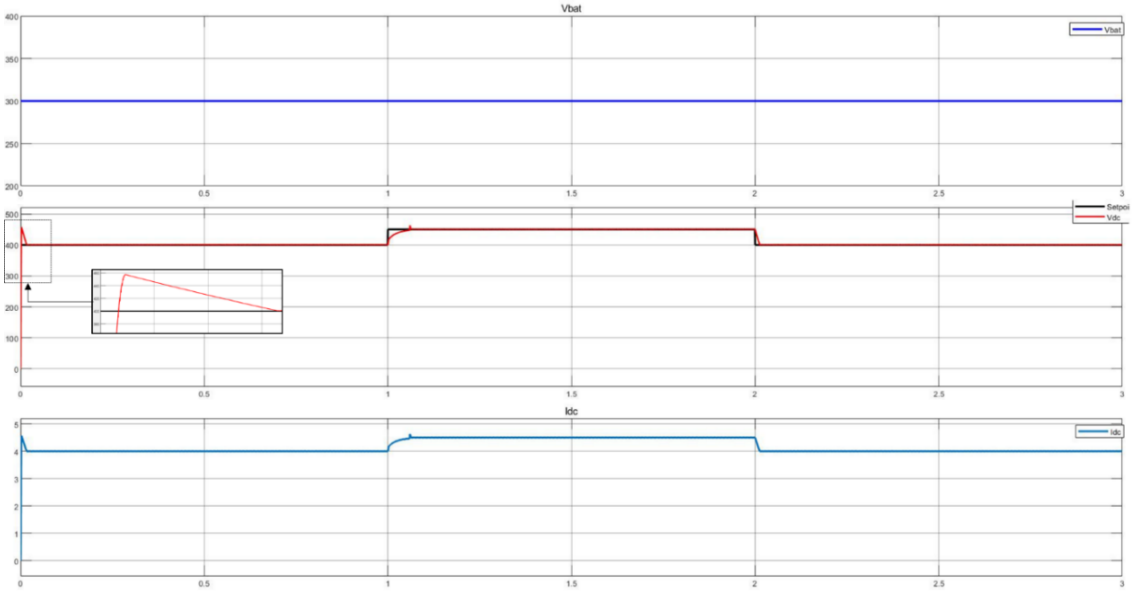

Fig. 12. Result in boost mode under FLC

5. CONCLUSION

This paper investigates a non-isolated buck-boost converter that enables bidirectional power flow, making it suitable for V2G and G2V applications. To evaluate its performance, a comprehensive simulation was conducted using MATLAB Simulink, comparing the effectiveness of a conventional PI controller and a FLC. The comparison between the PI controller and the FLC in both buck and boost modes highlights the superior performance of

the FLC in terms of response time, stability, and robustness. In buck mode, the FLC achieves a significantly faster rise time (0.38 ms vs. 1.66 ms) and a much shorter settling time (1 ms vs. 10 ms) compared to the PI controller, while also demonstrating high robustness to voltage sag. Similarly, in boost mode, the FLC outperforms the PI controller with a lower overshoot (14.38% vs. 19.4%) and a drastically reduced settling time (15 ms vs. 77 ms), making it more responsive to setpoint changes. Despite these enhancements, both controllers maintain steady-state accuracy with minimal error, particularly the PI controller, which can be beneficial for applications that require precise voltage regulation. Overall, the FLC proves to be a more efficient and adaptive control strategy for this bidirectional DC/DC converter, making it particularly suitable for applications like EV charging systems. While future research could explore its integration with RES to further enhance efficiency and reliability and investigate performance under dynamic and real-world operating conditions.

REFERENCES

[1] GARCIA A., MONSALVE-SERRANO J., VILLALTA D., TRIPATHI S., 2022, *Electric Vehicles Vs E-Fuelled ICE Vehicles: Comparison of Potentials for Life Cycle CO_2 Emission Reduction*, presented at the WCX SAE World Congress Experience, 2022-01–0745, https://doi.org/10.4271/2022-01-0745.

[2] INCI M., SAVRUN M.M., CELIK Ö., 2022, *Integrating Electric Vehicles as Virtual Power Plants: A Comprehensive Review on Vehicle-To-Grid (V2G) Concepts, Interface Topologies, Marketing and Future Prospects*, J. Energy Storage, 55, 105579.

[3] GOLLA N.K., SUDABATTULA S.K., 2021, *Withdrawn: Impact of Plug-in Electric Vehicles on Grid Integration with Distributed Energy Resources: A Comprehensive Review on Methodology of Power Interaction and Scheduling*, Mater. Today Proc., S2214785321023567, https://doi.org/10.1016/j.matpr.2021.03.306.

[4] HEYDARI-DOOSTABAD H., O'DONNELL T., 2022, *A Wide-Range High-Voltage-Gain Bidirectional DC–DC Converter for V2G and G2V Hybrid EV Charger*, IEEE Trans. Ind. Electron., 69/5, 4718–4729, https://doi.org/10.1109/TIE.2021.3084181.

[5] VADI S., BAYINDIR R., COLAK A.M., HOSSAIN E., 2019, *Review on Communication Standards and Charging Topologies of V2G and V2H Operation Strategies*, Energies, 12/19, 3748, https://doi.org/10.3390/en12193748.

[6] RAJENDRAN G., VAITHILINGAM C.A., MISRON N., NAIDU K., AHMED M.R., 2021, *A Comprehensive Review on System Architecture and International Standards for Electric Vehicle Charging Stations*, J. Energy Storage, 42, 103099.

[7] GOWDA C.K, KHEDEKAR V.G., ANANDH N., PARAGOND L.R.S., KULKARNI P., 2019, *Bidirectional on-Board EV Battery Charger with V2H Application*, Innovations in Power and Advanced Computing Technologies (i-PACT), Vellore, India: IEEE, 1–5, https://doi.org/10.1109/i-PACT44901.2019.8960126.

[8] SHARMA A., SHARMA S., 2019, *Review of Power Electronics in Vehicle-to-Grid Systems*, J. Energy Storage, 21, 337–361.

[9] TASNIM M.N., et al., 2024, *A Critical Review on Contemporary Power Electronics Interface Topologies to Vehicle-to-Grid Technology: Prospects, Challenges, and Directions*, IET Power Electron., 17/1, 157–181, https://doi.org/10.1049/pel2.12618.

[10] PANCHANATHAN S., et al., 2023, *A Comprehensive Review of the Bidirectional Converter Topologies for the Vehicle-to-Grid System*, Energies, 16/5, 2503.

[11] GORJI S.A., SAHEBI H.G., EKTESABI M., RAD A.B., 2019, *Topologies and Control Schemes of Bidirectional DC–DC Power Converters: an Overview*, IEEE Access, 7, 117997–118019, https://doi.org/10.1109/ACCESS.2019.2937239.

[12] WAGHMARE T., CHATURVEDI P., 2020, *Study of Bidirectional DC-DC Converter: Control Schemes and Switching Techniques*, in 2020 IEEE First International Conference on Smart Technologies for Power, Energy and Control (STPEC), Nagpur, India: IEEE, 1–6, https://doi.org/10.1109/STPEC49749.2020.9297713.

[13] AMIN A.A., ABDULLAH M., 2022, *A Comparative Study of DC-DC Buck, Boost, and Buck-Boost Converters with Proportional-Integral, Sliding Mode, and Fuzzy Logic Controllers*, Recent Adv. Electr. Electron. Eng. Former. Recent Pat. Electr. Electron. Eng., 15/1, 75–91.

[14] AL-DABBAGH Z.A., SHNEEN S.W., HANFESH A.O., 2024, *Fuzzy Logic-Based PI Controller with PWM for Buck-Boost Converter*, J. Fuzzy Syst. Control, 2/3, 147–159.

[15] DARAZ A., BASIT A., ZHANG G., 2023, *Performance Analysis of PID Controller and Fuzzy Logic Controller for DC-DC Boost Converter*, PloS One, 18/10, p. e0281122.

[16] NETHAJI G., KATHIRVELAN J., 2024, *Performance Comparison Between PID and Fuzzy Logic Controllers for the Hardware Implementation of Traditional High Voltage DC-DC Boost Converter*, Heliyon, 10/17, Available: https://www.cell.com/heliyon/fulltext/S2405-8440(24)12781-8,

[17] SUTIKNO T., APRILIANTO R.A., PURNAMA H.S., 2023, *Application of Non-Isolated Bidirectional DC–DC Converters for Renewable and Sustainable Energy Systems: A Review*, Clean Energy, 7/2, 293–311, https://doi.org/10.1093/ce/zkac070.

[18] TYTELMAIER K., HUSEV O., VELIGORSKYI O., YERSHOV R., 2016, *A Review of Non-Isolated Bidirectional Dc-Dc Converters for Energy Storage Systems*, in 2016 II International Young Scientists Forum on Applied Physics and Engineering (YSF), Kharkiv, Ukraine: IEEE, 22–28, https://doi.org/10.1109/YSF.2016.7753752.

[19] SARIF M.S.M., PEI T.X., ANNUAR A.Z., 2018, *Modeling, Design and Control of Bidirectional DC-DC Converter Using State-Space Average Model*, in IEEE Symposium on Computer Applications & Industrial Electronics (ISCAIE), Penang, Malaysia: IEEE, 416–421, https://doi.org/10.1109/ISCAIE.2018.8405509.

[20] ATACAK I., BAY O.F., 2012, *A Type-2 Fuzzy Logic Controller Design for Buck and Boost DC–DC Converters*, J. Intell. Manuf., 23/4, 1023–1034, https://doi.org/10.1007/s10845-010-0388-1.

[21] BHOWATE A., DEOGADE S., 2016, *Comparison of PID Tuning Techniques for Closed Loop Controller of Dc-Dc Boost Converter*, Conference: 6th International Conference on Intelligent and Advanced Systems (ICIAS), https://doi.org/10.1109/ICIAS.2016.7824044.

[22] BORASE R.P., MAGHADE D.K., SONDKAR S.Y., PAWAR S.N., 2021, *A Review of PID Control, Tuning Methods and Applications*, Int. J. Dyn. Control, 9/2, 818–827, https://doi.org/10.1007/s40435-020-00665-4.

[23] AC R., REDDY V.S., 2025, *Bidirectional DC-DC Converter Circuits and Smart Control Algorithms: a Review*, Available: https://papers.ssrn.com/sol3/papers.cfm?abstract_id=4255850.

[24] SADOLLAH A., 2018, *Introductory Chapter: which Membership Function is Appropriate in Fuzzy System?*, in Fuzzy Logic Based in Optimization Methods and Control Systems and its Applications, A. Sadollah, Ed., InTech, https://doi.org/10.5772/intechopen.79552.

[25] MAMDANI E.H., ASSILIAN S., 1975, *An Experiment in Linguistic Synthesis with a Fuzzy Logic Controller*, Int. J. Man-Mach. Stud., 7/1, https://doi.org/10.1016/S0020-7373(75)80002-2.

[26] PRECUP R.-E., HELLENDOORN H., 2010, *A Survey on Industrial Applications of Fuzzy Control*, Comput. Ind., 62/3, 213–226, https://doi.org/10.1016/j.compind.2010.10.001.

[27] ROSS T.J., 2010, *Fuzzy Logic with Engineering Applications*, 3rd ed. Chichester, U.K: John Wiley, https://doi.org/10.1002/9781119994374.

[28] JANG J.-S.R., SUN C.-T., MIZUTANI E., SUN C., 1997, *Neuro-Fuzzy and Soft Computing: A Computational Approach to Learning and Machine Intelligence*, in MATLAB curriculum series. Upper Saddle River, NJ: Prentice Hall.